Journal of Power Sources 210 (2012) 303–320

Contents lists available at SciVerse ScienceDirect

Journal of Power Sources

journal homepage: www.elsevier.com/locate/jpowsour

System simulation of compressed hydrogen storage based residential wind hybrid power systems

Mandhapati Raju [a], Siddhartha Kumar Khaitan [b,*]

[a] Convergent Science Inc., Middleton, WI 53562, United States
[b] Iowa State University, Electrical and Computer Engineering Department, Ames, IA 50014, United States

ARTICLE INFO

Article history:
Received 10 December 2011
Received in revised form 13 February 2012
Accepted 15 February 2012
Available online 28 March 2012

Keywords:
Compressed hydrogen storage
Small wind system
Wind turbine
Electrolyzer
Fuel cell
Redlich–Kwong gas equation

ABSTRACT

This paper deals with the storage of excess wind energy, in a hybrid wind power system, in the form of compressed hydrogen. A system simulation model is developed in Matlab/Simulink platform for the charging and discharging dynamics of compressed hydrogen storage system integrated with the wind turbine and the fuel cell. Wind model is used to estimate the power generation in the wind turbine. When the wind power generation exceeds the load, the excess power is diverted to the electrolyzer to produce hydrogen. As and when the pressure inside the electrolyzer builds, a compressor is operated intermittently (for higher efficiency) to divert the hydrogen into high pressure cylinders. When demand exceeds the power generation, fuel cell supplies the power to the load. A number of fuel cell stacks are provided to meet the required load. The overall efficiency of the storage system, defined as the ratio of the useful energy derived from the storage system to the energy diverted to the storage system is found to be 24.5% for the compressed hydrogen storage based system.

1. Introduction

Wind power has been proposed to be technically viable for different applications. Storage of excess wind power in the form of hydrogen [1] is an attractive alternative. Hydrogen provides for storage and transportation of energy storage at a much higher energy density [2]. Typical hydrogen storage density is 123 MJ kg^{-1} compared to Gasoline (47.2 MJ kg^{-1}) and Diesel (45.4 MJ kg^{-1}). Effective storage of hydrogen is the key in wind energy–hydrogen storage based hybrid power generation systems. Different storage options [3–9] including compressed hydrogen storage and metal hydride based hydrogen storage have been proposed for the wind hybrid systems. For small scale residential applications compressed hydrogen storage is a straightforward option for storing hydrogen that is produced from renewable energy sources. The design of compressed hydrogen storage has much less infrastructure requirements [10] compared to the other storage options like metal hydride, chemical hydride, cryo-adsorption etc. Depending on the operating pressure of the storage tank, a suitable compressor has to be chosen and the storage tank has to be designed to withstand the operating pressure with extra safety allowances. No elaborate heating or cooling arrangements need to be provided.

1.1. Research relevant to compressed hydrogen storage systems

Researchers have proposed the integration of compressed hydrogen storage systems [11,12] in connection with wind power to achieve large penetration of wind energy. Electrolyzers can be used as controllable loads [13,14] within the power system to achieve high penetrations of wind power. A theoretical investigation of the wind energy–hydrogen storage based system has been conducted [15] and a procedure to evaluate the efficiency of the wind energy conversion system is presented. A theoretical discussion is provided for the choice of the operating parameters for different components to achieve maximum efficiency. However, the storage system is not modeled and the efficiency of the system is not presented.

Zhou and Francois [16] conducted control oriented modeling of the electrolyzer for the hydrogen storage process. Hydrogen from the electrolyzer is compressed into a tank. Electrolyzer is modeled in sufficient detail but a simplified model of a compressed storage system is used by assuming the temperature of the tank to be constant. Their primary emphasis was to control the different physical quantities to ensure efficient and reliable operation of the electrolyzer. Onar et al. [12] presented a detailed dynamic model, design and simulation of wind/fuel cell/ultra capacity based hybrid power generation system. They have shown that the system can handle variable wind speed and load requirements. However, compressed storage model is simplified by assuming a constant temperature and by neglecting the

* Corresponding author. Tel.: +1 515 2945499; fax: +1 515 2944263.
E-mail address: siddhartha.khaitan@gmail.com (S.K. Khaitan).

0378-7753/$ – see front matter © 2012 Elsevier B.V. All rights reserved.
doi:10.1016/j.jpowsour.2012.02.050

Nomenclature

Wind parameters

v_w	upstream wind velocity ($m\,s^{-1}$)
A	swept area of the rotor blades
ρ	density of air ($kg\,m^{-3}$)
C_p	performance coefficient
λ	tip speed ratio
θ	pitch angle (radians)
ω	rotational speed of rotor blades (s^{-1})
R	radius of the rotor blades (m)
P_{avg}	average power generated by the turbine

Electrolyzer parameters

N_{el}	number of electrolyzers
I_{el}	current through the electrolyzer (A)
u_{el}	utilization factor (0.9)
ΔH_c	heat of combustion of hydrogen
P_{el}	electrical power consumed by the electrolyzer
F	Faraday's constant
A_e	area of the electrodes (m^2)
$\dot{n}_{in}$	rate of electrolyzer production ($mol\,s^{-1}$)
$\dot{n}_{out}$	rate of hydrogen flux into the storage bed ($mol\,s^{-1}$)
P_{el}	electrical power consumed by the electrolyzer (W)
P_{th}	thermal power generated by the electrolyzer (W)
r, s, t	electrolyzer parameters
V_{el}	voltage across the electrolyzer
V	volume of the buffer space in the electrolyzer (m^3)

Fuel cell parameters

A_{st}	area of the fuel cell stack (m^2)
I_{st}	current through the stack (A)
N_{st}	number of stacks
n_{fc}	number of fuel cells per stack
ΔG_f	change in Gibbs free energy at standard pressure (1 bar)
ΔG_f°	change in Gibbs free energy
$\bar{R}$	universal gas constant ($8.314\,J\,mol^{-1}\,K^{-1}$)
T_{fc}	temperature of the fuel cell (K)
p	partial pressure (bar)
v_{act}	activation voltage (V)
v_0	voltage drop at zero current density (V)
v_a	constant
c_1	constant
v_{ohm}	voltage drop due to ohmic loss (V)
v_{conc}	voltage drop due to concentration losses (V)
R_{ohm}	ohmic resistance (Ω)
c_2, c_3, i_{max}	constants
v_{fc}	voltage of single fuel cell (V)
v_{st}	voltage of the stack (V)

Hydrogen storage parameters

a, b	Redlich–Kwong coefficients
$c_{p,g}$	specific heat of hydrogen gas ($J\,kg^{-1}\,K^{-1}$)
$c_{p,m}$	specific heat of storage container material ($J\,kg^{-1}\,K^{-1}$)
$\dot{m}_s$	mass flow rate of hydrogen supply ($kg\,s^{-1}$)
p	bed pressure (Pa)
P	design safety pressure (=2.25p) (Pa)
r_i	inner radius of the container (m)
t	time (s)
t_h	thickness of container (m)
T	temperature of the bed (K)
T_{amb}	temperature of the ambient (K)
U	heat transfer coefficient ($W\,m^{-2}\,K^{-1}$)
UTS	ultimate tensile strength (ksi)
A	area of heat transfer (m^2)
v	specific molar volume ($m^3\,mol^{-1}$)
V_{bed}	volume of the storage bed (m^3)
V_m	volume of the storage container material (m^3)
Z	compressibility factor
ρ_g	density of hydrogen in the gas phase ($kg\,m^{-3}$)
ρ_m	density of storage container material ($kg\,m^{-3}$)

Compressor parameters

P_1	compressor inlet pressure (bar)
P_2	compressor outlet pressure (bar)
T_2	compressor outlet temperature (K)
T_2	compressor outlet temperature (K)
P_{comp}	compressor power (W)
n	polytropic expansion coefficient

compression energy and compressor dynamics. A techno-economic analysis [17] of the hourly management of the energy generated in wind–hydrogen systems has been conducted. The efficiency of the electricity–hydrogen–electricity conversion is estimated to be around 30%. In reality, the incorporation of real gas effects and compressor power will lead to a lower prediction of the system efficiency. Ref [6] provides an excellent review of the modeling of the different components of the renewably driven hydrogen storage systems.

1.2. Motivation for the current research

To the authors' knowledge, typical modeling of compressed hydrogen storage systems for wind hybrid applications assumes ideal gas behavior of hydrogen and also neglects the heat generated during compression. At high pressures, hydrogen deviates from ideal gas behavior significantly. Compressibility factor is a thermodynamic property which quantifies the modification of the ideal gas law to account for real gas behavior. Fig. 1 shows the variation of compressibility factor of hydrogen gas in the pressure range of 1 bar to 200 bar and the temperature range of 270 K to

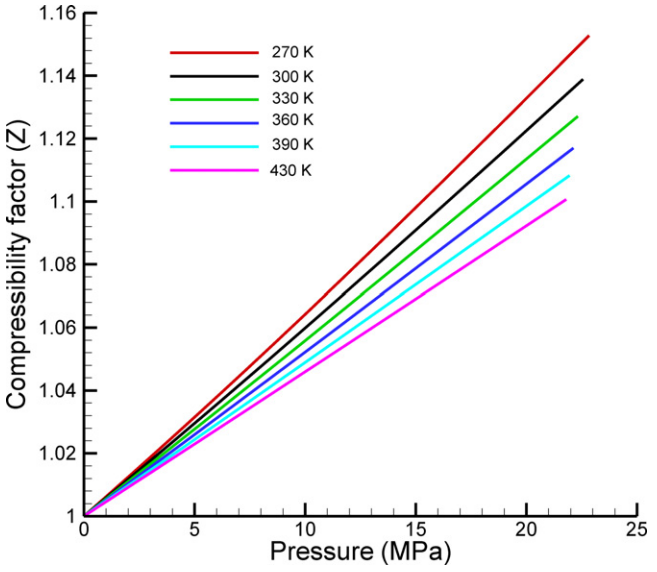

Fig. 1. Variation of compressibility factor of hydrogen gas with pressure and temperature.

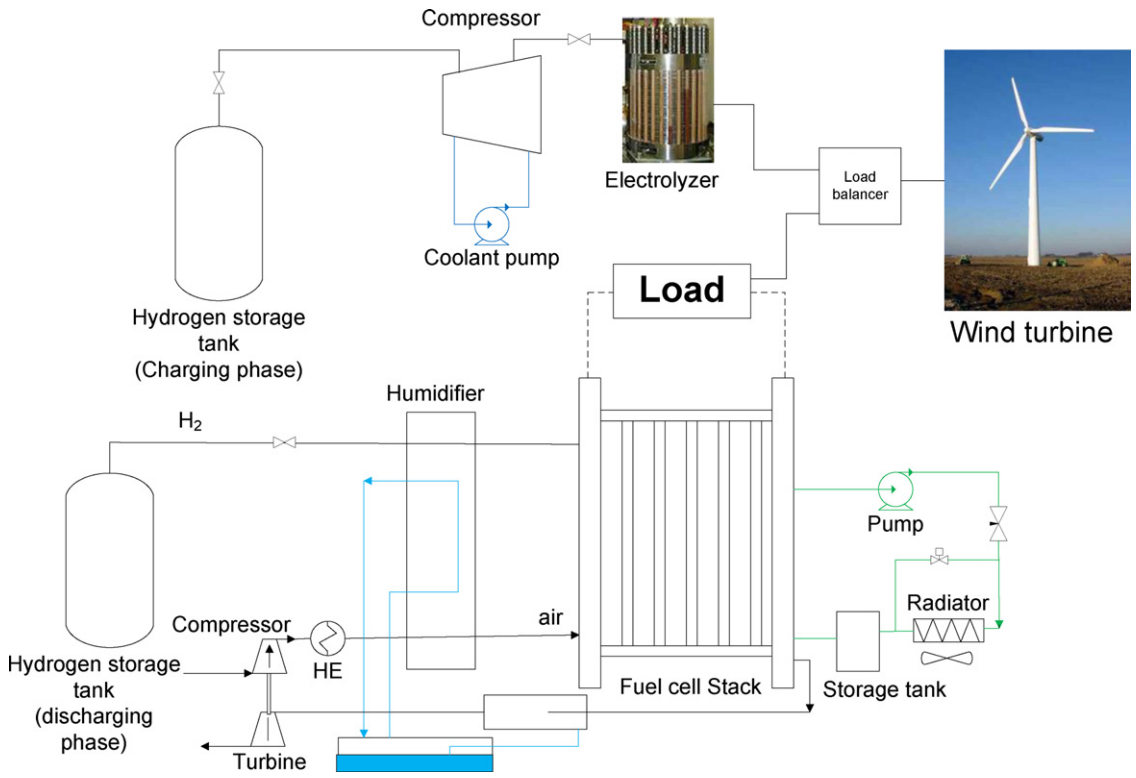

Fig. 2. Schematic of wind–fuel cell-compressed hydrogen storage system.

430 K. At low pressures (around 50 bar), the compressibility factor is around 1.02. Hence the deviation from the ideal gas is only 2%, which is considered negligible. However, as the pressure increases, the compressibility factor increases. At pressures around 200 bar (and temperature 300 K), the compressibility factor is around 1.2, which implies a deviation of around 20% from the ideal gas behavior. Hence, for compressed storage technology where the storage pressure is designed to operate at a pressure of 100–200 bar, the real gas effects become important. To consider the real gas effects, Redlich–Kwong [18] equation is taken. The heat of compression is taken into account by solving the energy balance equation. The amount of hydrogen stored in tank not only depends on the pressure inside the tank but also the temperature of the gas. For storage applications, where faster rates of refueling are required (as in the case of automobile vehicles), the temperature rise inside the tank could be quite high during refueling [19], necessitating some cooling arrangement to ensure proper refueling. In the case of wind energy based hydrogen production, the refueling rate is not very high. However, there will still be reasonable temperature variation in the storage tank. The temperature variation will reduce the storage capacity of the tank. For example if the temperature of the tank increases during refueling, the net amount of hydrogen stored in the tank at a given pressure decreases. Similarly, if the temperature of the gas reduces during discharging, the residual amount of gas left inside the tank at a specified cut off pressure increases. Hence the net storage capacity of the tank decreases.

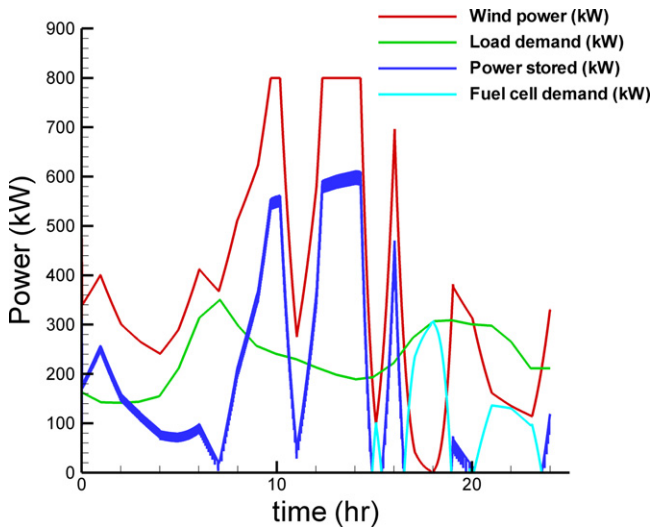

Fig. 3. Wind power and load management curve. (For interpretation of the references to color in the text citation of this figure, the reader is referred to the web version of the article.)

In the case of compressed storage system, the dynamics of the operation of the compressor and the storage system is important to consider. The operation of a compressor is a key factor in determining the efficiency of the storage system. This topic has not been sufficiently addressed in the literature. Continuous operation of the compressor will significantly lower the efficiency of the storage system and its life span. The renewable energy source being intermittent, hydrogen is not continuously produced and so

Table 1
Wind turbine characteristics.

Parameter	Value	Units
Height of the wind turbine	80	m
Diameter of the turbine	40	m
Maximum performance coefficient	0.59	
Cut-in speed	3	$m\,s^{-1}$
Cut-out turbine power	800	kW

the compressor will have to run idle, at times, when hydrogen is not generated. A more suitable option is to run the compressor intermittently, whenever required. A buffer space can be provided where the hydrogen from the electrolyzer can be rerouted. The pressure in this buffer storage can be allowed to increase to a certain level, after which the compressor starts its operation. During compressor operation, the pressure inside the buffer will decrease. Once the pressure drops to a certain level, compressor operation is stopped and hydrogen is allowed to collect in the buffer. This intermittent operating of the compressor will increase the efficiency of the system. However, the compressor should be able to operate intermittently without degrading its performance.

In this paper, a generalized overview of the working of a hydrogen storage system for small wind residential applications is presented, which include electrolyzer for producing hydrogen and a fuel cell to generate electricity from the hydrogen. Both charging and discharging dynamics are presented in this paper based on Matlab/Simulink simulations. During the charging simulation, compressor is in operation. During discharging, fuel cell is in operation. The dynamics of the compressor operation, fuel cell operation and the storage bed are presented in detail for a typical residential wind energy application.

2. Wind–fuel cell configuration

The wind–fuel cell hybrid configuration consists of a wind turbine generator and a fuel cell connected to a load bus. Wind turbine generates electricity and is connected to the load bus. This will supply the load demand. Fig. 2 shows the wind–fuel cell–hydrogen storage hybrid configuration. Since wind energy is intermittent and is subject to very high transient variation, any excess power generated by the turbine over the load is transferred to the electrolyzer to generate hydrogen. This hydrogen is then sent to a compressed storage tank using a compressor. Two storage modules are provided. One will be operating in charging mode and the other will be operating in the discharging mode. Whenever the turbine power cannot meet the load requirements, the fuel cell comes into operation. Depending on the power requirements on the fuel cell, the fuel cell would demand sufficient amount of hydrogen from the bed. The bed in the discharging mode will provide the hydrogen to the fuel cell. The capacity of the storage bed is chosen such that it

Table 2
Voltage coefficients of the electrolyzer.

Parameter	Value	Units
r_1	8.24×10^{-5}	$\Omega\,m^2$
r_2	-4.12×10^{-7}	$\Omega\,m^2\,{}^\circ C^{-1}$
s_1	0.2393	V
s_2	−0.002952	$V^\circ\,C^{-1}$
s_3	1.55×10^{-5}	$V^\circ\,C^{-2}$
t_1	0.6767	$A^{-1}\,m^2$
t_2	−0.02711	$A^{-1}\,m^2\,{}^\circ C^{-1}$
t_3	0.0004856	$A^{-1}\,m^2\,{}^\circ C^{-2}$
t_4	-2.69×10^{-6}	$A^{-1}\,m^2\,{}^\circ C^{-3}$

Table 3
Fuel cell parameters.

Number of cells per stack	800
Reversible cell voltage	0.95 V
Operating temperature	60 °C
Cut-off pressure	3 bar

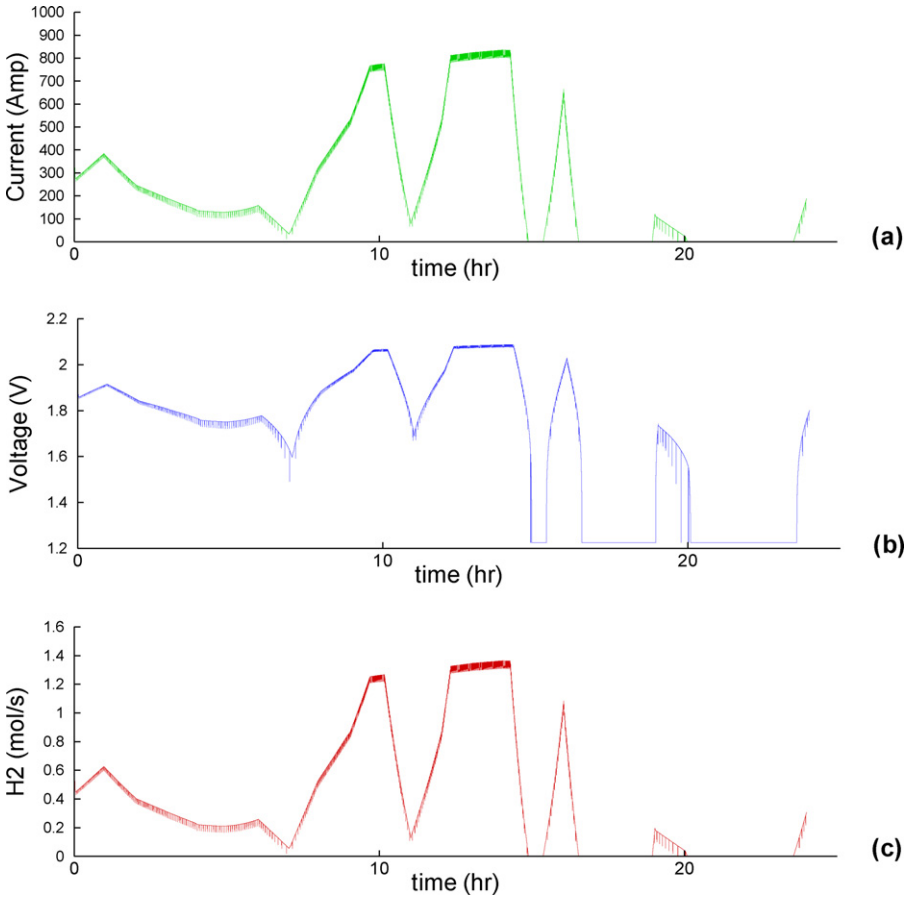

Fig. 4. Electrolyzer performance curve.

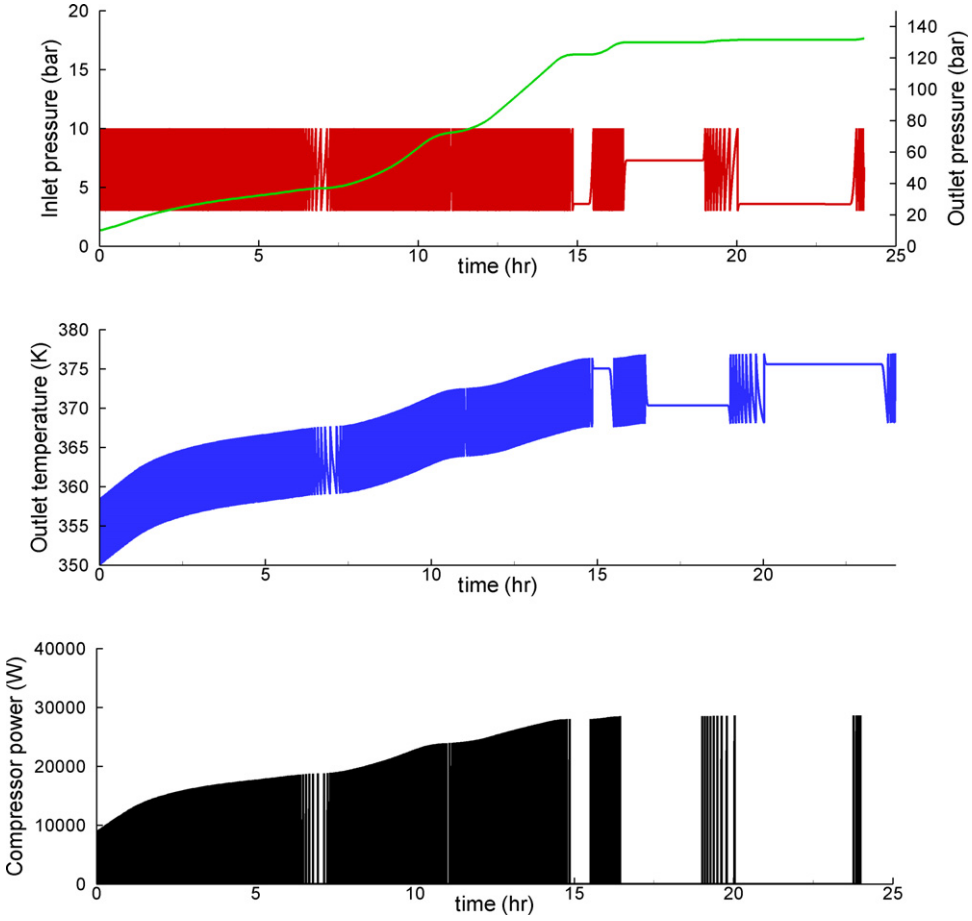

Fig. 5. Compressor performance curves.

can store all the hydrogen generated from the excess wind power for a single day operation based on the wind velocity and load demand curves chosen in this study. This method could in general be extended to estimate the storage bed capacity for continuous operation throughout the year based on the weather forecast and the load demand forecast analysis.

3. Wind turbine model

The power generated by the wind turbine is given as [20,21]

$$P_{\text{avg}} = \frac{1}{2}\rho C_{\text{p}} A v_{\text{w}}^3 \tag{1}$$

$$C_{\text{p}}(\lambda, \theta) = 0.73\left(\frac{153}{\lambda_i} - 0.38\theta - 0.002\theta^{2.14} - 13.2\right)e^{-18.4/\lambda_i} \tag{2}$$

$$\lambda_i = \frac{1}{\lambda - 0.02\theta} - \frac{0.003}{\theta^3 + 1} \tag{3}$$

The tip speed ratio is given as

$$\lambda = \frac{\omega R}{v_{\text{w}}} \tag{4}$$

Table 1 shows the characteristics of the wind turbine. The performance coefficient has a maximum value of 0.59. The cut-in speed is taken as 3 m s^{-1} and the cut-out turbine power is 800 kW. The wind turbine will not generate any useful power if the wind speed is below this cut-in speed.

4. Electrolyzer

The model developed by Artuso et al. [22] is used to simulate an advanced KOH alkaline electrolyzer. A total of 350 such electrolyzer units are provided to generate hydrogen from the excess power. The characteristic equation for this model is given as

$$V_{\text{el}} = U_{\text{ref}} + \frac{r}{A}I_{\text{el}} + s\left(\log\left(\frac{t}{A}I_{\text{el}} + 1\right)\right) \tag{5}$$

The ohmic resistance r, parameters s and t are functions of temperatures as given below

$$r = r_1 + r_2 T \tag{6}$$

$$s = s_1 + s_2 T + s_3 T^2 \tag{7}$$

$$t = t_1 + t_2 T + t_3 T^2 + t_4 T^3 \tag{8}$$

The coefficients in Eqs. (6)–(8) are given in Table 2. The area of the electrodes A is taken as 0.25 m^2 and the reversible cell voltage is taken as 1.229 V [23].

The relationship between the produced hydrogen molar flow rate and the current applied to the electrolyzer is given by

$$\dot{n}_{\text{el}} = \frac{N_{\text{el}} I_{\text{el}} u_{\text{el}}}{2F} \tag{9}$$

The utilization factor [24] is taken as 0.9.

The electrical power P_{el} consumed by the electrolyzer is given as

$$P_{\text{el}} = N_{\text{el}} V_{\text{el}} I_{\text{el}} \tag{10}$$

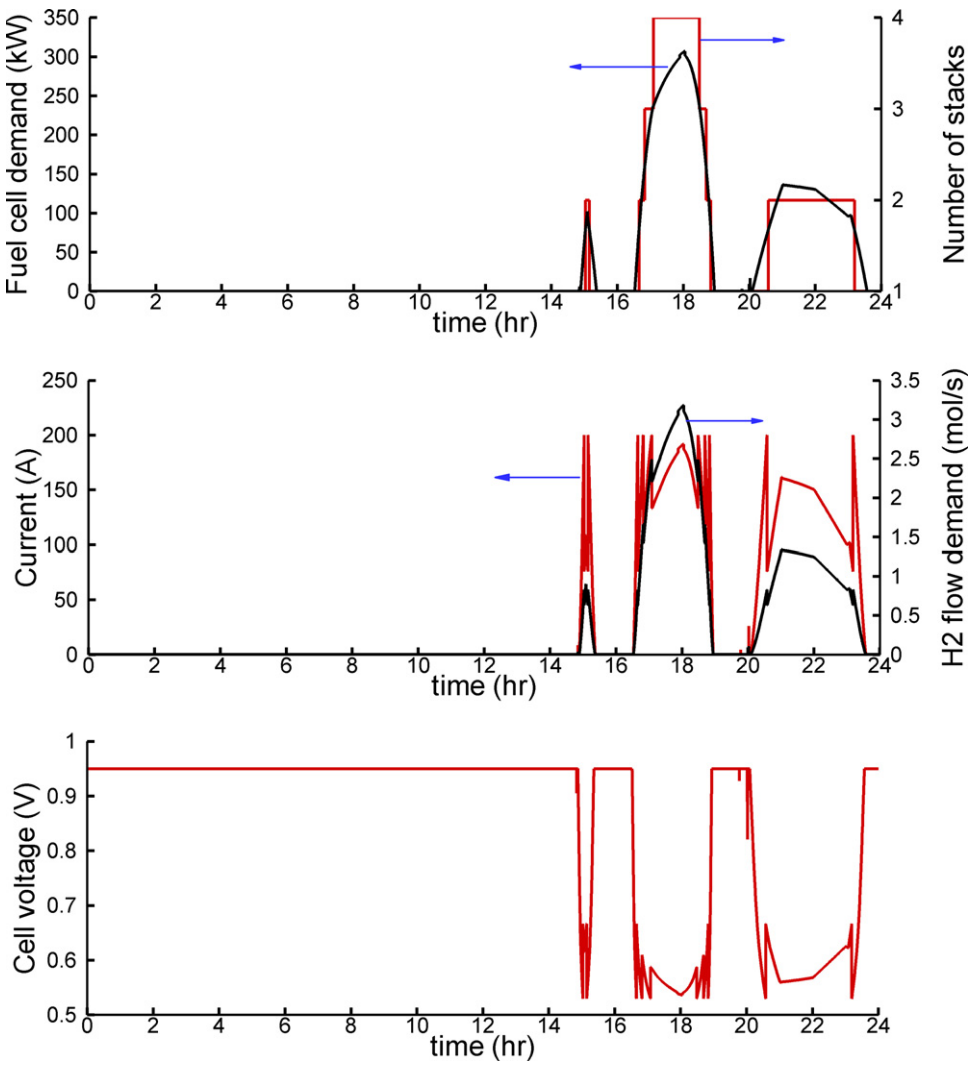

Fig. 6. Fuel cell demand, current and voltage curves.

The thermal power P_{th} generated by the electrolyzer is given by the following equations

$$P_{th,el} = P_{el} - \dot{n}_{el}\,\Delta H_c \tag{11}$$

The thermal power generated can be calculated from Eq. (11). In this paper, detailed modeling is not presented for the thermal management of the electrolyzer. Rather it is assumed that a coolant is supplied which can effectively remove this heat generated during electrolyzer operation to maintain a constant temperature of 80 °C, which is the operating temperature of the electrolyzer. In reality, the temperature of the electrolyzer will slightly vary during the operation, which would in turn affect the amount of hydrogen generated from the electrolyzer. This effect is neglected in this paper.

5. Compressed hydrogen storage model

To study the dynamics of the compressed hydrogen storage, the governing equations of the mass and energy balance is considered along with the real gas equation.

5.1. Mass balance

Mass balance states that the net mass influx of hydrogen (mass inflow rate – mass outflow rate) will cause an increase in the density of hydrogen inside the storage bed as given by the following equation

$$\dot{m}_s = V_{bed}\frac{d\rho_g}{dt} \tag{12}$$

5.2. Energy balance

Energy balance conserves the total energy within the storage bed as given by the following equation.

$$(\rho_g c_{p,g} V_{bed} + \rho_m c_{p,m} V_m)\frac{dT}{dt} = UA(T_{amb} - T) + V_{bed}\frac{dp}{dt} + \dot{m}_s c_{p,g}(T_{in} - T) \tag{13}$$

In Eq. (13), the first term in the left hand side (LHS) represents the net increase in the internal energy of the storage bed (which includes the hydrogen gas and the storage tank material). The first term in the right hand side (RHS) represents the heat transfer from the ambient to the storage bed. Usually this term is small and is neglected. The second term in the RHS represents the heat of compression. During compression, the temperature of the gas rises and similarly during expansion, the temperature of the gas falls down. The third term in the RHS represents the convective heat transfer from the inflowing hydrogen.

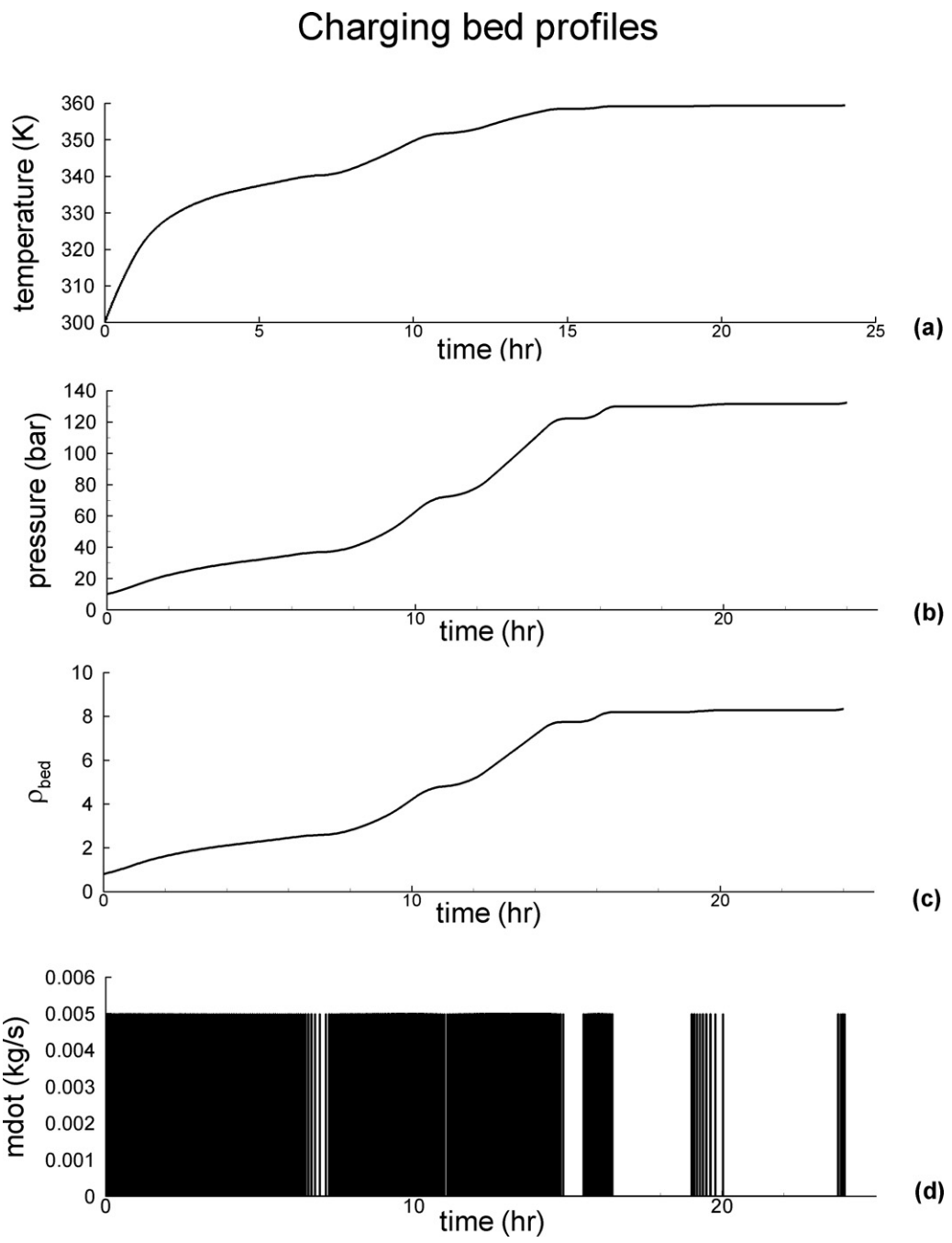

Fig. 7. Charging bed profiles.

5.3. Redlich–Kwong gas equation

Since hydrogen deviates from ideal gas behavior at high pressure, the use of ideal gas equation will lead to significant deviation. Eq. (15) represents the Redlich–Kwong equation used to account for the real gas effect. The compressibility factor can be estimated based on Eq. (15).

$$P = \frac{RT}{v-b} - \frac{a}{\sqrt{T}v(v+b)} \tag{14}$$

$$Z = \frac{Pv}{RT} \tag{15}$$

5.4. Storage tank thickness calculations

The allowable stress [25] used to determine the minimum storage container wall thickness is based on the tensile and yield strength of the material.

$$t_h = \frac{r_i P}{UTS - 0.6P} \tag{16}$$

316L stainless steel of 75 ksi ultimate tensile strength is chosen as the container material.

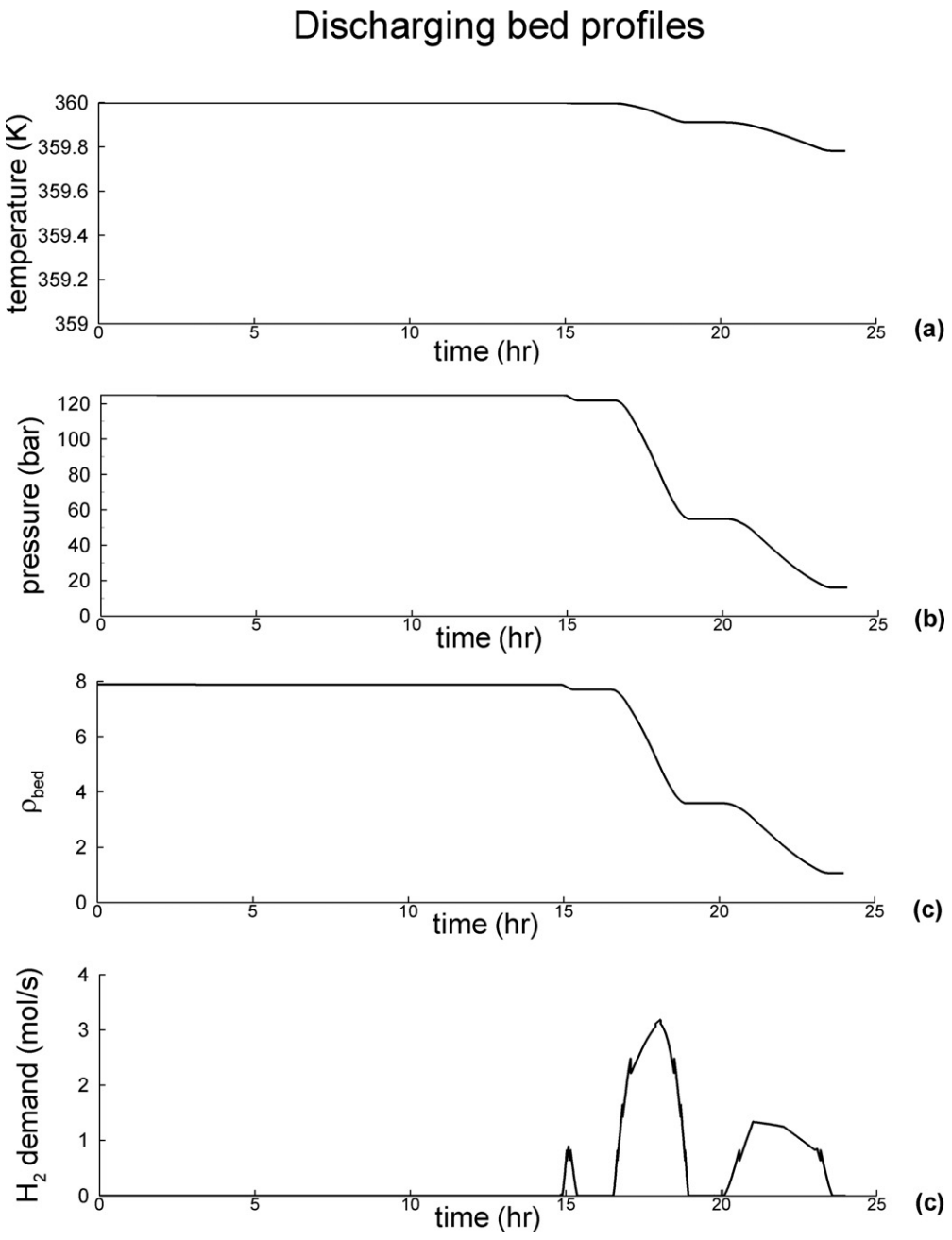

Fig. 8. Discharging bed profiles.

6. Compressor model

For a real gas, the polytropic compression work can be approximated as [26]

$$P_{\text{comp}} = \dot{m}_s R T_1 Z_1 \frac{n}{n-1}\left(\left(\frac{P_2}{P_1}\right)^{(n-1)/n} - 1\right) \tag{17}$$

7. Fuel cell model

A Proton Exchange Membrane (PEM) based fuel cell is used. The PEM fuel cell model is taken from Pukrushpan et al. [27,28]. The equations for the fuel cell models are presented below.

Fuel cell open circuit voltage

$$\Delta G_f = \Delta G_f^{\circ} - \bar{R} T_{fc} \ln\left[\frac{p_{H_2} {p_{O_2}}^{1/2}}{p_{H_2O}}\right] \tag{18}$$

Reversible voltage of the fuel cell

$$E = \frac{\Delta G_f}{2F} \tag{19}$$

$$i = \frac{I_{st}}{A_{st}} \tag{20}$$

Cell terminal voltage

$$v_{fc} = E - v_{act} - v_{ohm} - v_{conc} \tag{21}$$

$$v_{fc} = E - (v_0 + v_a(1 - e^{-c_1 i})) - (iR_{ohm}) - \left(i\left(c_2 \frac{i}{i_{max}}\right)^{c_3}\right) \tag{22}$$

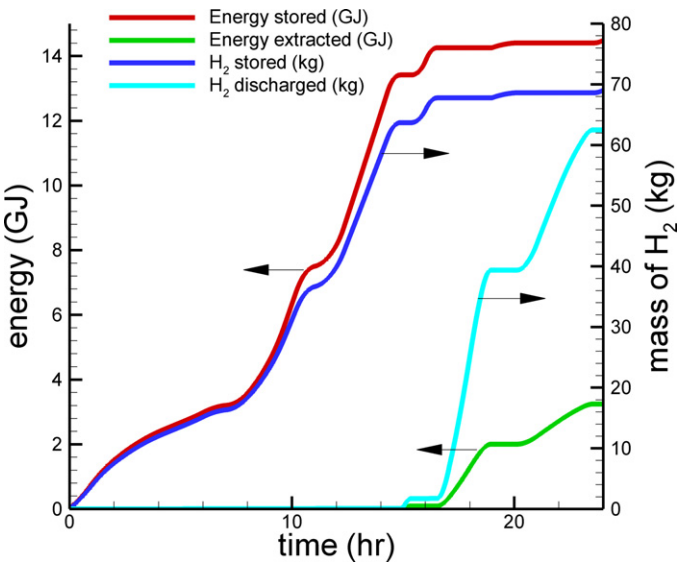

Fig. 9. Energy management curves. (For interpretation of the references to color in the text citation of this figure, the reader is referred to the web version of the article.)

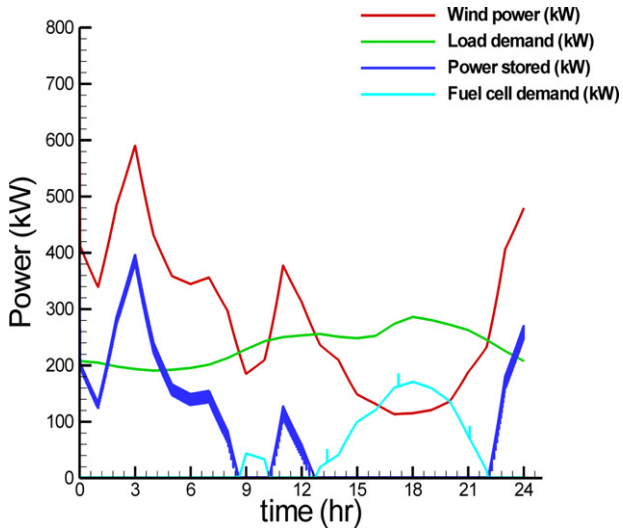

Fig. 11. Wind power and load management curve for a typical winter day. (For interpretation of the references to color in the text citation of this figure, the reader is referred to the web version of the article.)

$$v_{st} = n \times v_{fc} \tag{23}$$

The reversible cell voltage is taken as 0.95 V. Table 3 shows the fuel cell characteristics. A number of fuel cell stacks are provided. Each fuel cell stack consists of 800 fuel cells.

8. Results and discussion

Fig. 3 shows the wind power generated (red line) from the wind turbine. This wind power is obtained from the wind model (Section 3). The wind velocity is chosen for a location at Deer Lodge, MT on March 12, 2007 [29]. The wind turbine is designed to generate a maximum output of 800 kW. The green line shows a typical load curve for a residential application [29]. The blue line shows the excess power directed towards storage. Note that the compressor operation requires power and this power comes from the wind turbine. The blue line actually indicates the net power (wind power generated–load demand power–compressor power) directed to the electrolyzer. Note that the blue line shows oscillations. This is due to the intermittent operation of the compressor during

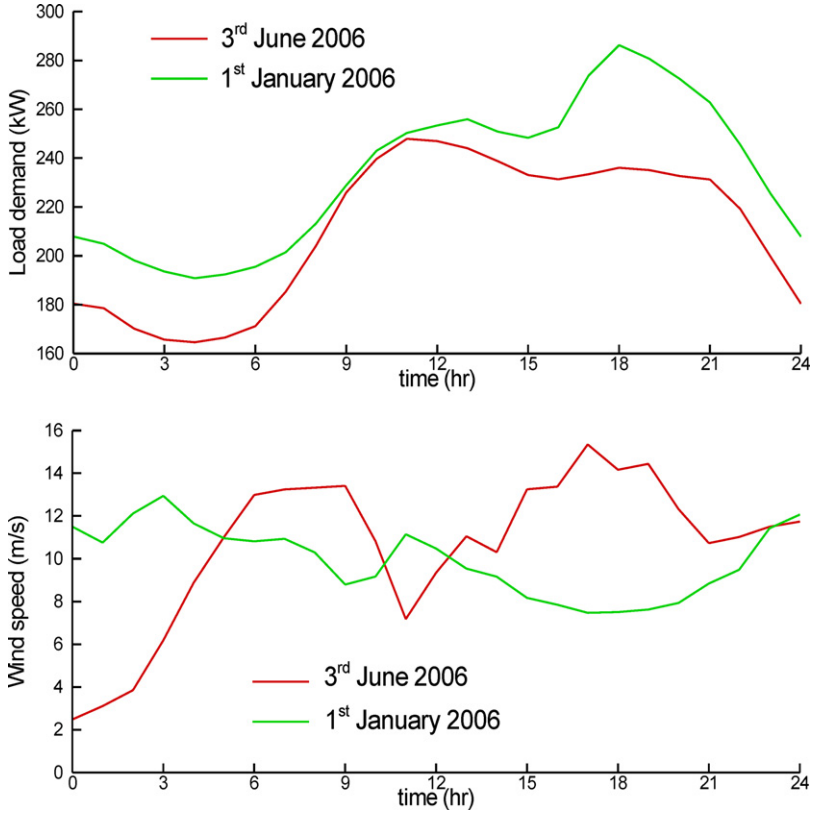

Fig. 10. Load demand and wind speed profiles on a typical summer and winter day.

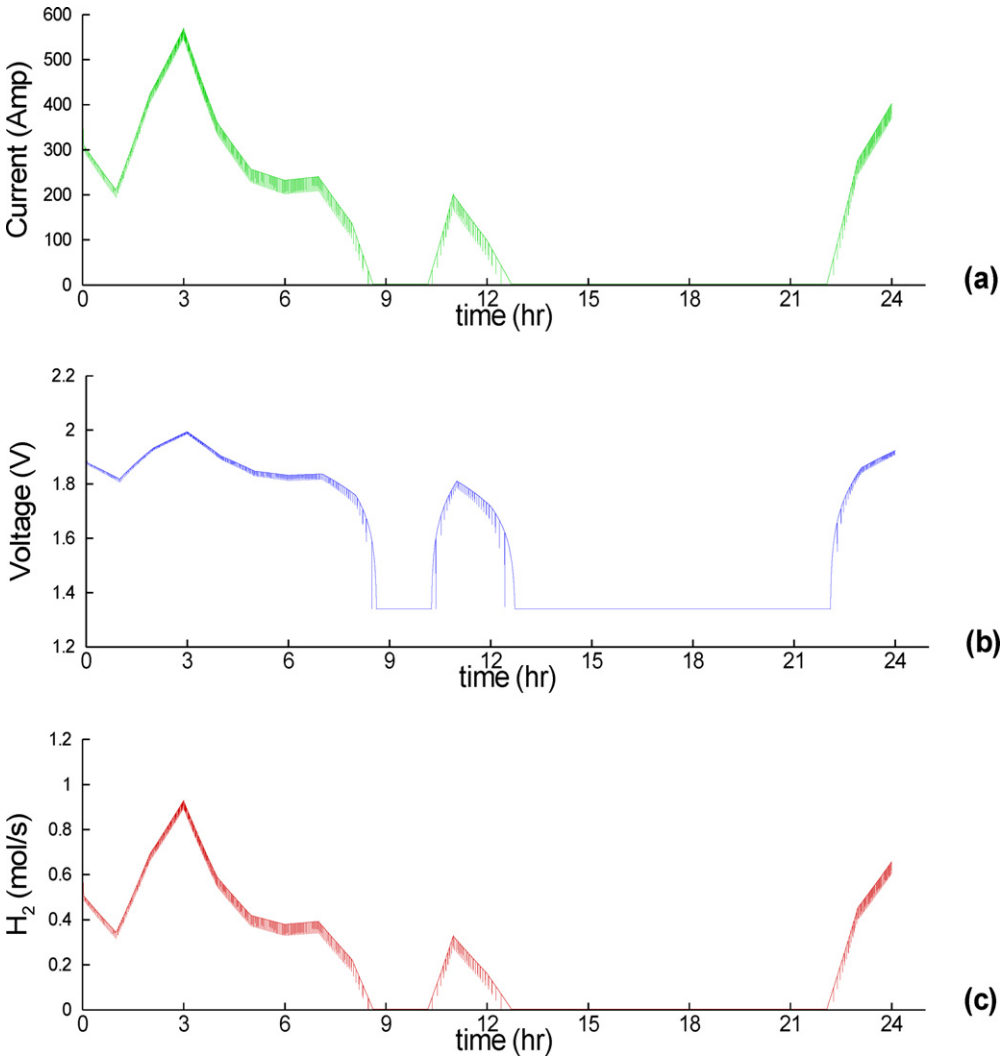

Fig. 12. Electrolyzer performance curves for a typical winter day.

charging. The cyan line shows the power demanded by the load from the fuel cell. All the energy generation/demand is translated to/from hydrogen via a storage tank. Fig. 3 shows that most of the time, wind turbine produces excess power. Only in the last few hours shown in the plot, there is a power demand from the fuel cell.

Electrolyzer performance is determined based on Eqs. (5)–(10). Fig. 4 shows the performance of the electrolyzer based on the excess input power supplied by the wind turbine (see blue line in Fig. 3). Based on the power input, the current (Fig. 4(a)) and the voltage profiles vary (Fig. 4(b)). The oscillations in the current and the voltage profiles are due to the oscillations in the excess wind power diverted to the electrolyzer. The temperature of the electrolyzer is fixed at 350 K. The hydrogen production is a function of the current flowing through the electrolyzer and hence its variation (Fig. 4(c)) is similar to that of the current flowing through the electrolyzer. Now this hydrogen evolving out of the electrolyzer builds up pressure in the electrolyzer. The pressure in the electrolyzer/buffer is allowed to increase up to 10 bar. When the pressure exceeds 10 bar, compressor begins to operate. When the compressor begins to operate, hydrogen is removed out from the electrolyzer buffer, causing the pressure of the electrolyzer to decrease. Compressor operation is stopped, when the pressure in the electrolyzer reaches 3 bar. The pressure in the electrolyzer is dependent on the net difference between the rate of production of hydrogen in the electrolyzer and on the rate of hydrogen removal by the compressor. Thus, the electrolyzer buffer pressure is given by the equation

$$\frac{dp}{dt} = Z\frac{\dot{n}_{in} - \dot{n}_{out}}{V}RT \tag{24}$$

where $\dot{n}_{in}$ is the number of mole produced by the electrolyzer, $\dot{n}_{out}$ is the number of moles entering the storage bed, V is the volume of the buffer space (taken as 100 l) either in the electrolyzer or that of a separate buffer storage tank, if provided and T is the temperature of the electrolyzer.

Fig. 5 shows the operation of the electrolyzer/compressor system. By using intermittent operation of the compressor, energy is conserved by not having to run the compressor at times, when there is no hydrogen production. The pressure of the electrolyzer is maintained in the range of 3–10 bar. The compressor is rated to compress 5 g s^{-1} of hydrogen to maximum pressure of 125 bar. The compressor inlet pressure is the electrolyzer pressure and the compressor outlet pressure is the bed pressure. Both the inlet pressure and the outlet pressure varies dynamically with time and hence the compressor power varies dynamically. Fig. 5(a) shows

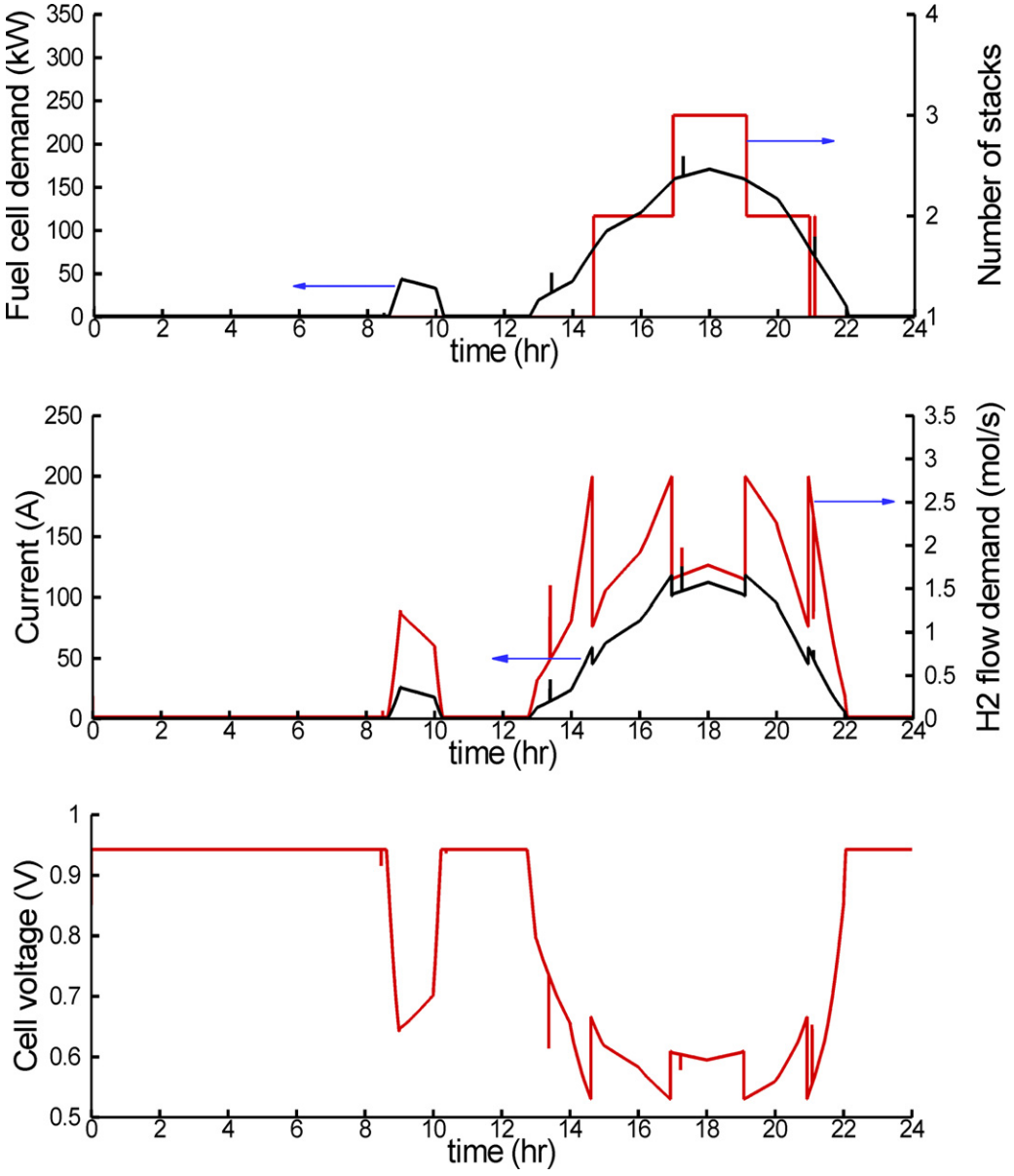

Fig. 13. Fuel cell performance curves for a typical winter day.

the inlet (electrolyzer) and the outlet (bed) pressure. Compressor draws power from the wind turbine directly. But if the wind turbine is not able to supply the necessary power, fuel cell supplies the power to the compressor. Note that the temperature of the hydrogen gas at the inlet of the compressor is that of the electrolyzer temperature (350 K). Fig. 5(b) shows the compressor outlet temperature. Compression is assumed to be a polytropic process with a polytropic coefficient of 1.02 (nearly isothermal). The compressor is operated at a near isothermal process (by using a coolant) to reduce the power consumption. Fig. 5(c) shows the compressor power. The compressor power oscillates due to the variation in the pressure ratio between the inlet and the outlet. The average power consumption rises due to the increase in the outlet (bed) pressure as the bed is getting filled up.

Fig. 6 shows the dynamic performance of the fuel cells during their operation. Fig. 6(a) shows the load demand requested from the fuel cell and the number of fuel cell stacks in operation. As the load demand increases, more stacks come into operation. For a multiple stack operation, the load is equally distributed amongst all the stacks. Fig. 6(a) shows that a maximum of four stacks are set into operation. Fig. 6(b) shows the stack current in Amperes. The abrupt variation in the stack current is due to the fact that the number of stacks in operation is changing. If the number of stacks changes, then the load requested per fuel cell stack will change. Correspondingly, the stack current also changes. Moreover, the efficiency of the stack changes with the change in power. This will also affect the stack current. Fig. 6(c) shows the individual cell voltage. The fuel cell delivers 0.95 V at no-load operation. During load conditions, the fuel cell voltage drops.

A total of 50 storage beds each of length 1 m, inner diameter 0.426 m and thickness 7.4 mm are in operation. The thickness of the bed is designed to operate at a maximum pressure of 125 bar. The number of beds and the size of each bed are chosen to meet the requirements of the hydrogen production during charging and

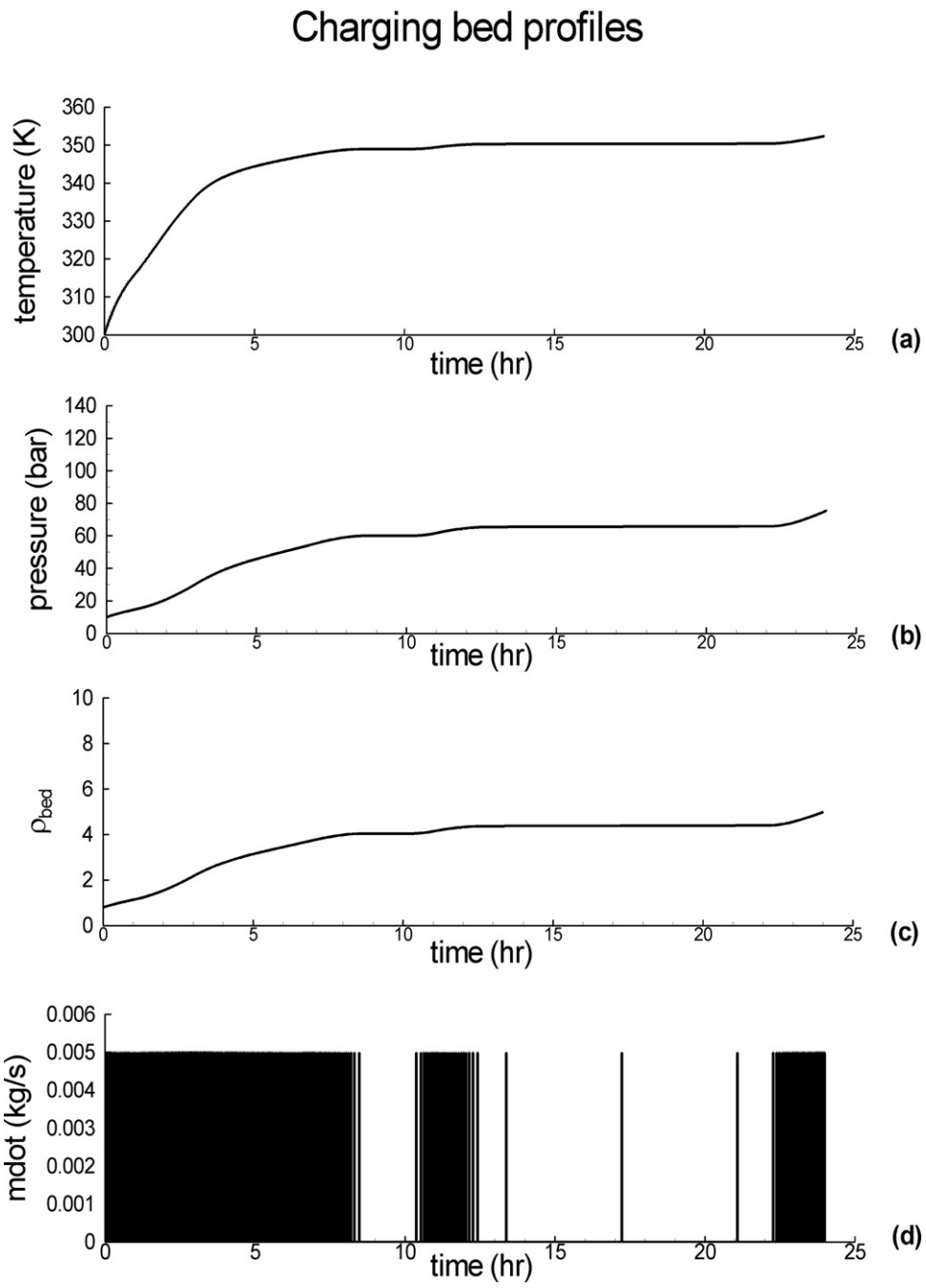

Fig. 14. Charging profiles for storage bed for a typical winter day.

the hydrogen demand during discharging. All the beds are charged simultaneously. Fig. 7 shows the performance of the storage system during charging based on Eqs. (12)–(15). Fig. 7(a) shows variation of temperature of the storage bed. The temperature of the bed increases monotonically due to the heat of compression and convective heating from the incoming hydrogen gas. Note that the temperature of the incoming hydrogen gas is always above 350 K. During times, when there is no supply of hydrogen from the compressor, the temperature of the bed remains fairly constant. During other times when there is continuous supply of hydrogen from the compressor, the temperature of the bed rises sharply. Fig. 7(b) and (c) shows the variation of the pressure and density of hydrogen gas in the bed. Fig. 7(d) shows the mass flow rate of the incoming hydrogen gas from the compressor. Since the operation of the compressor is intermittent, the mass flow rate varies as a step function between 0 and 5 g s^{-1}.

Fig. 8 shows the performance of the storage bed during discharge. All the beds are equally discharged. The bed temperature is assumed to be initially at 360 K. The temperature of the bed falls when hydrogen is removed from the bed by the cooling effect produced due to expansion. The pressure (Fig. 8(b)) and the density of the bed (Fig. 8(c)) decreases as hydrogen is removed out of the bed. Fig. 8(d) shows the mass flow demand from the fuel cell.

Fig. 9 shows the energy distribution in the wind/fuel cell/hydrogen storage hybrid system. The red line shows the

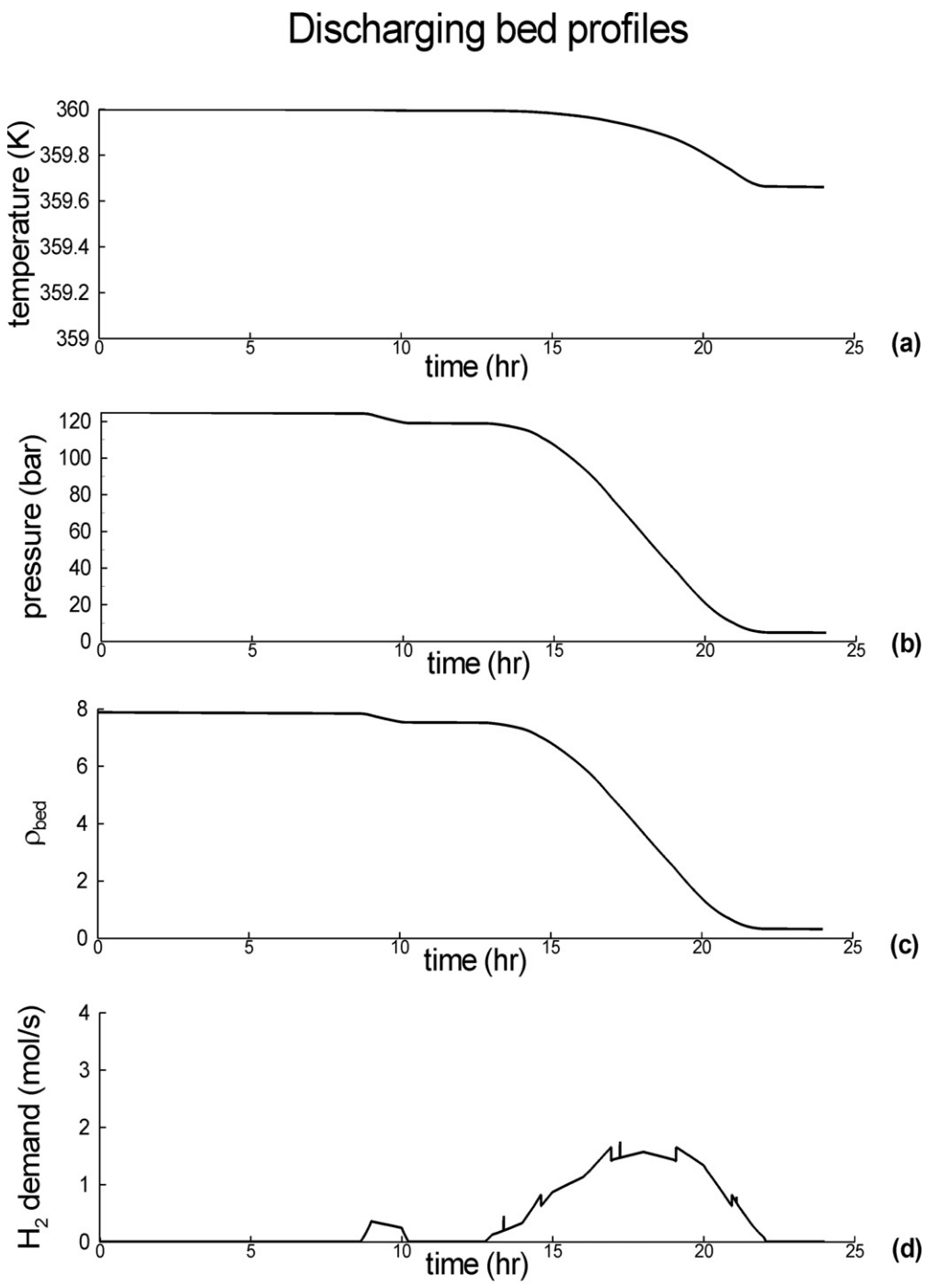

Figure 15: Discharging profiles of the storage bed for a typical winter day

Fig. 15. Discharging profiles of the storage bed for a typical winter day.

cumulative energy that is diverted from the wind turbine to the electrolyzer for storage. Cumulative energy is obtained by integrating the instantaneous power. By the end of 24 h, a total of around 14.4 GJ of wind energy is diverted for storage. With this energy, a total of 69 kg of hydrogen (blue line) is generated by the electrolyzer. Based on the load demand, a total of 3.2 GJ of energy is extracted from the storage for meeting the load requirements. To meet this load demand, a total of 62.5 kg of hydrogen is consumed. This figure gives a rough idea of the efficiency of the storage system. For more accurate estimation, the energy required to produce 62.5 kg of hydrogen is calculated as $62.5 \times (14.4/69) = 13.04$ GJ of energy. Correspondingly, when 62.5 kg of hydrogen is consumed, a total of 3.2 GJ of energy can be extracted from the fuel cell. This gives an overall storage efficiency of $(3.2/13.04) \times 100 = 24.5\%$ for this compressed hydrogen storage system. This implies that if 100 units of energy are sent for storage, only 24.5 units of that stored energy can be extracted. The remaining energy is lost as thermal heat losses in the electrolyzer, fuel cell, compressor

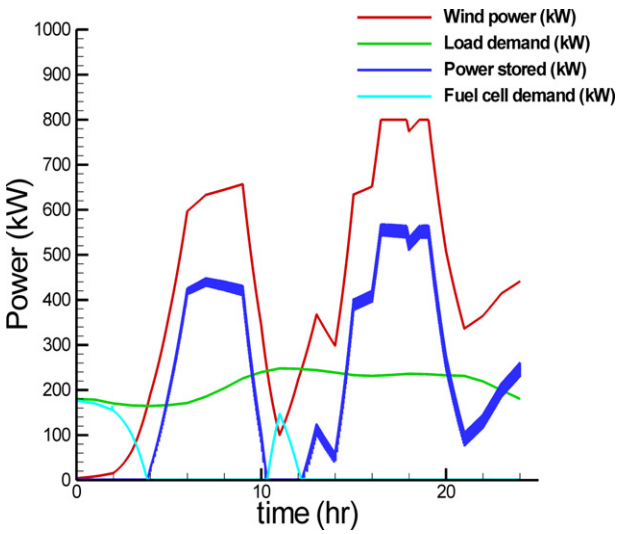

Fig. 16. Wind and load management curves for a summer day. (For interpretation of the references to color in the text citation of this figure, the reader is referred to the web version of the article.)

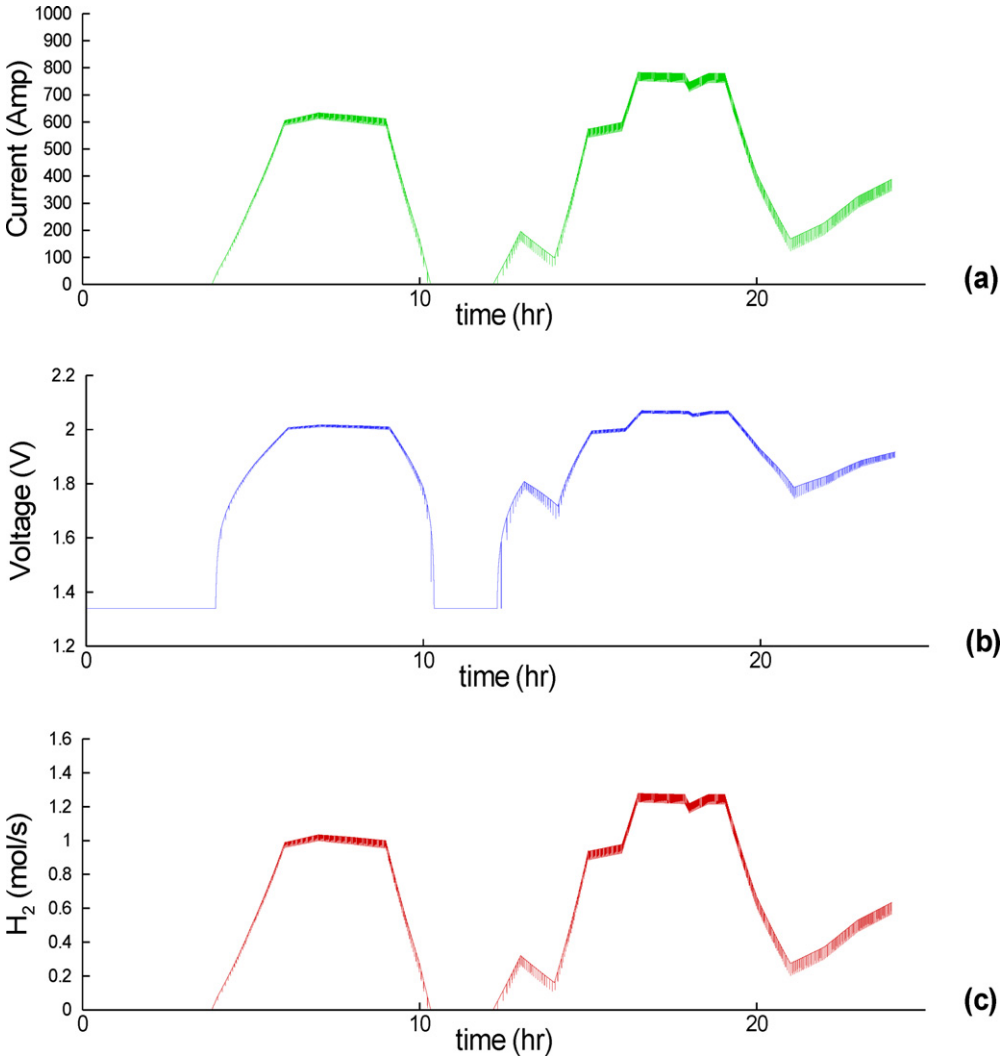

Fig. 17. Electrolyzer performance curves for a typical summer day.

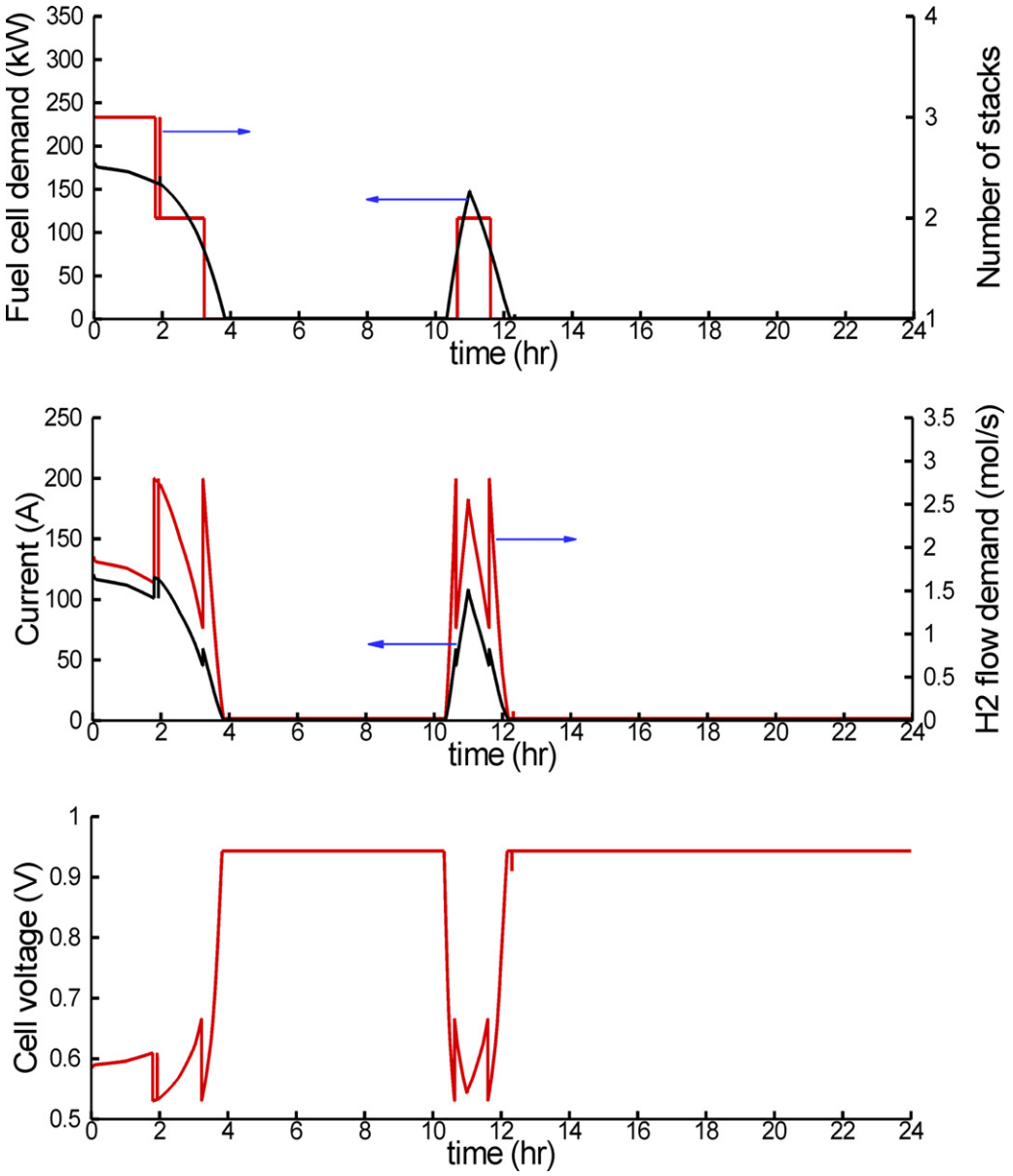

Fig. 18. Fuel cell performance curves for a typical summer day.

losses and other losses. The estimation of overall storage efficiency will help the designer to design the size of the storage system and the wind turbine capacity for a given residential load. The next section shows the performance of the system with seasonal variation.

8.1. Seasonal performance

To study the behavior of the system at different seasons, wind speed and load demand data is taken on a typical summer day (3rd June 2006) and a typical winter day (1st January 2006) at a particular location at Maine. The load demand data is obtained from the public website [30]. Note that the load demand is for the entire town which is reported in MWH. The load is appropriately scaled down to the current system. The wind speed data is obtained from NREL public domain website [31] for the same region. Fig. 10 shows the wind speed and the load demand profiles for both the days. As seen in Fig. 10, peak summer load is in the afternoon and the peak winter load is in the evening.

8.2. System performance on a winter day:

Fig. 11 shows the wind power generated (red line) from the wind turbine for a typical winter day. The load demand curve is shown in green line. As shown in the figure, wind power is minimal at around 6 pm and the load is maximum around 6 pm. Hence there is peak demand from fuel cell at around 6 pm. Wind power generation is maximum at around 3 am. Hence the electrolyzer load is maximum at around 3 am. Figs. 12 and 13 show the electrolyzer performance curves and the fuel cell performance curves respectively. From the figures it is clear that the peaks in the electrolyzer and fuel cell performance curves follow the peaks in the wind generation and load demand curves respectively. Figs. 14 and 15 show the charging bed and the discharging bed performance curves.

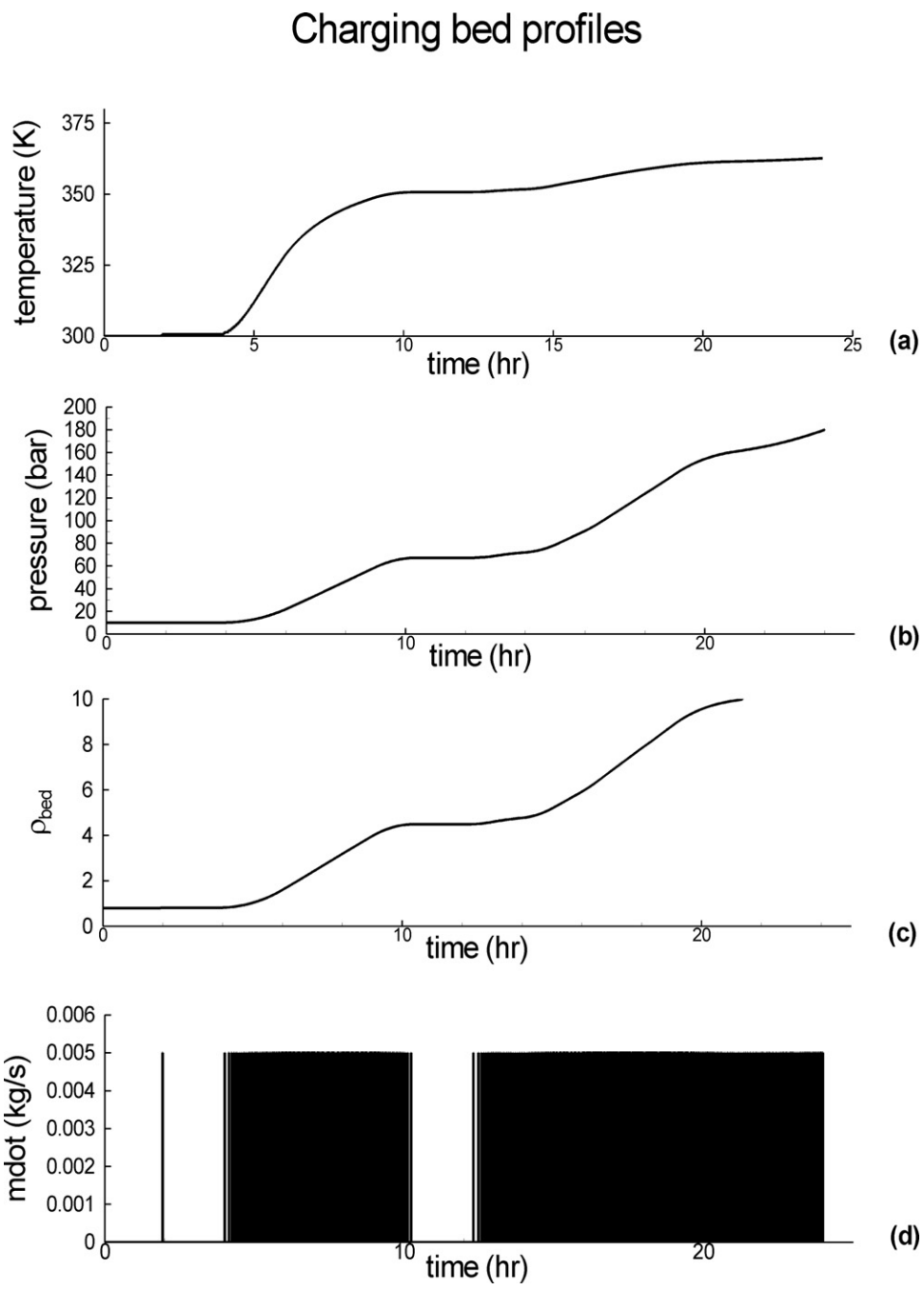

Fig. 19. Charging profiles for storage bed for a typical summer day.

8.3. System performance on a summer day

Fig. 16 shows the wind power generated (red line) and the load demand (green line) on a typical summer day. As shown in the figure, the wind power generation on this particular day is maximum in the range of 4–8 pm. On this particular day, the wind speed is quite high and hence greater load is transferred to the electrolyzer for storage. The load demand is maximum at around 11 am and remains high during the day time till 8 pm. Figs. 17 and 18 show the electrolyzer performance curves and the fuel cell performance curves respectively. Similarly Figs. 19 and 20 show the charging bed and the discharging bed performance curves. As shown in Fig. 19, the hydrogen generation is quite high due to high load on the electrolyzer. This leads to a rise in the bed pressure to around 180 bar. The bed is not designed to handle such high pressures and so the bed may have to be vented once the pressure exceeds the safety limit. Or else an extra storage module has to be provided to store the excess hydrogen once the first storage module is filled. As shown in Fig. 20, the load demand from the fuel cell is less and so the bed is not fully emptied by the end of the day. Effective power management strategies should be designed to handle such situations.

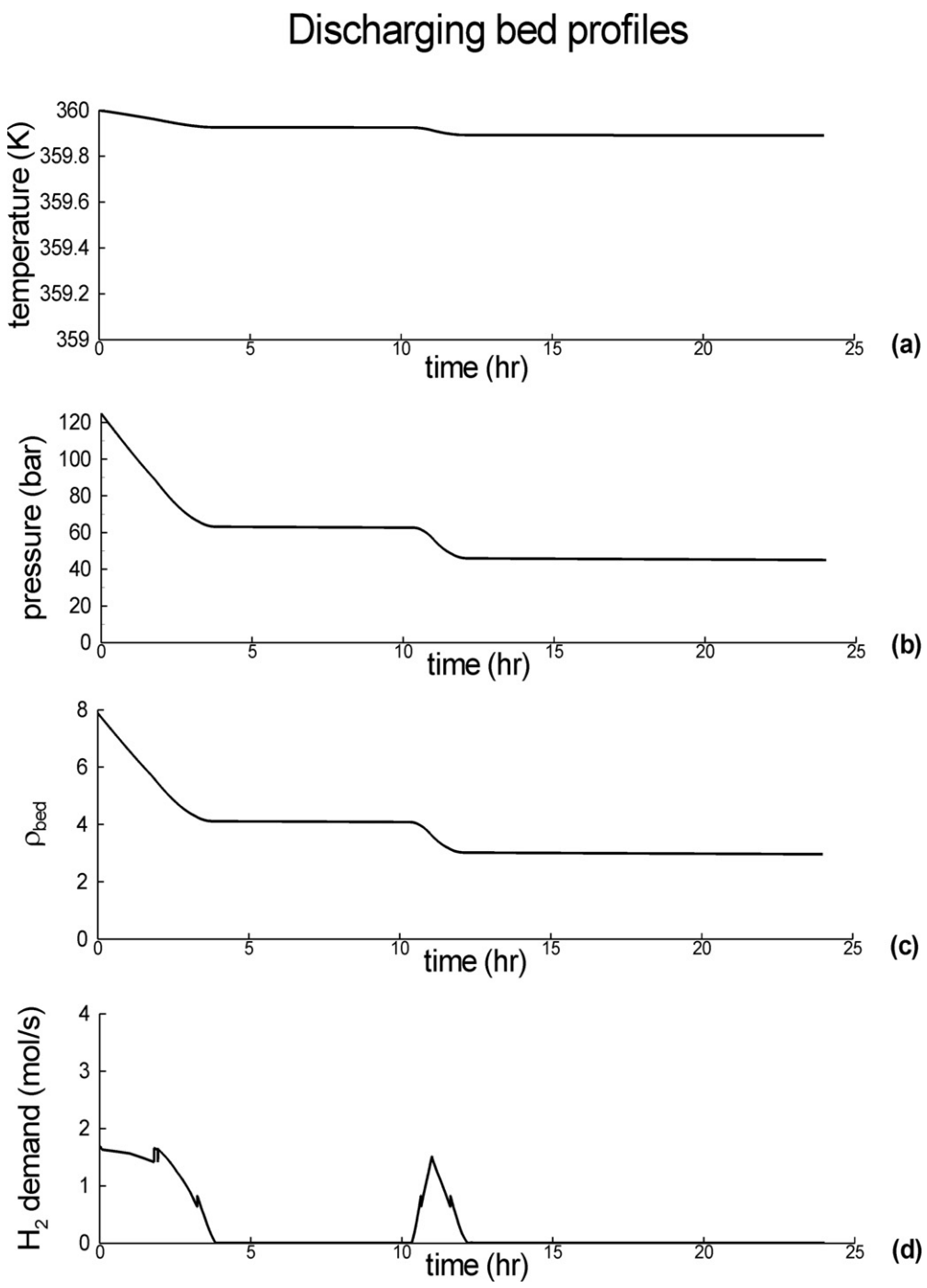

Fig. 20. Discharging profiles for storage bed for a typical summer day.

9. Conclusions

System level simulation is performed for a residential small wind hybrid system. Compressed hydrogen storage is used to store the hydrogen generated by the excess wind power. Hydrogen is generated by a total of 350 electrolyzer units. A compressor is used to compress hydrogen to a maximum pressure of 125 bar. A number of fuel cell stacks containing 800 cells per stack and supplying a maximum power of 80 kW are provided to meet the excess load demand. Separate storage beds are provided for charging and discharging. The compression energy for real gas is taken into account. Results are shown for a typical daily operation a wind turbine. An overall storage efficiency, defined as the ratio of the excess energy diverted to the storage to the useful energy extracted from the storage, is estimated to be around 24.5%. The value reported includes the compressor power for compressing hydrogen into the storage tank and the fuel cell air compressor power. However, the power required by the auxilary units like the coolant flow unit and the humidifier unit are neglected.

References

[1] I.F. Bitterlin, Journal of Power Sources 162 (2) (2006) 906–912.
[2] R. Dell, D. Rand, Journal of Power Sources 100 (1) (2001) 2–17.
[3] S.A. Sherif, F. Barbir, et al., Solar Energy 78 (5) (2005) 647–660.
[4] M. Raju, S. Khaitan, International Journal of Hydrogen Energy 36 (17) (2011) 10797–10807.

[5] S. Khaitan, M. Raju, International Journal of Hydrogen Energy 37 (3) (2012) 2344–2352.
[6] S.S. Deshmukh, R.F. Boehm, Renewable and Sustainable Energy Reviews 12 (9) (2008) 2301–2330.
[7] M. Little, M. Thomson, et al., International Journal of Hydrogen Energy 32 (10–11) (2007) 1582–1588.
[8] R. Gazey, S.K. Salman, D.D. Aklil-D'Halluin, Journal of Power Sources 157 (2006) 841–847.
[9] F.J. Pino, L. Valverde, F. Rosa, Journal of Power Sources 196 (2011) 4418–4426.
[10] J. Zheng, X., Liu, P., Xub, P., Liu, Y., Zhao, J. Yang, International Journal of Hydrogen Energy, in press.
[11] A. Gonzalez, E. McKeogh, B.O. Gallachoir, Renewable Energy 29 (4) (2003) 471–489.
[12] O.C. Onar, M. Uzunoglu, M.S. Alam, Journal of Power Sources 161 (2006) 707–722.
[13] E. Troncoso, M. Newborough, International Journal of Hydrogen Energy 32 (13) (2007) 2253–2268.
[14] H. De Battista, R.J. Mantz, F. Garelli, Journal of Power Sources 155 (2006) 478–486.
[15] W.J. Yang, O. Aydin, International Journal of Energy Research 25 (5) (2001) 449–463.
[16] T. Zhou, B. Francois, International Journal of Hydrogen Energy 34 (1) (2009) 21–30.
[17] J.L. Bernal-Agustín, R. Dufo-López, International Journal of Hydrogen Energy 33 (22) (2008) 6401–6413.
[18] O. Redlich, J.N.S. Kwong, Chemical Reviews 44 (1) (1949) 233–244.
[19] L. Zhao, Y. Liu, J. Yang, Y. Zhao, J. Zheng, H. Bie, X. Liu, International Journal of Hydrogen Energy 35 (15) (2010) 8092–8100.
[20] G.T. Son, H.J. Lee, J.W. Park, Industry Applications Society Annual Meeting. IEEE, 2009, pp. 1–8.
[21] E. Muljadi, C.P. Butterfield, IEEE Industry Applications Society Annual Meeting Phoenix, vol. 1, Arizona, 1999, pp. 323–330.
[22] P. Artuso, F. Zuccari, A. Dell'Era, F. Orecchini, Journal of Solar Energy Engineering 132 (3) (2010).
[23] Ø. Ulleberg, International Journal of Hydrogen Energy 28 (1) (2003) 21–33.
[24] J.P. Vanhanen, P.D. Lund, International Journal of Hydrogen Energy 20 (7) (1995) 575–585.
[25] E. Livingston, R.J. Scavuzzo, Pressure Vessels, The Engineering Handbook, CRC Press, Boca Raton, 2000.
[26] Harry Silla, Chemical Process Engineering: Design and Economics, CRC Press, 2003.
[27] J.T. Pukrushpan, A.G. Stefanopoulou, H. Peng, Control of Fuel Cell Power Systems: Principles, Modeling, Analysis and Feedback Design, Springer Verlag, 2004.
[28] J.T. Pukrushpan, H. Peng, A.G. Stefanopoulou, Journal of dynamic systems measurement and control 126 (14) (2004) 14–25.
[29] C. Wang, C.M. Colson, M.H. Nehrir, J. Li, Power Electronics and Machines in Wind Applications. IEEE PEMWA, 2009, pp. 1–7.
[30] http://www.iso-ne.com/markets/hrly_data/selectHourlyLoad.do.
[31] http://www.nrel.gov/wind/systemsintegration/ewits.html.